ELSEVIER

Journal of Structural Geology 28 (2006) 972–979

JOURNAL OF STRUCTURAL GEOLOGY

www.elsevier.com/locate/jsg

Uniform distribution of points on a hypersphere for improving the resolution of stress tensor inversion

Katsushi Sato *, Atsushi Yamaji

Division of Earth and Planetary Sciences, Graduate School of Science, Kyoto University, Kyoto 606-8502, Japan

Abstract

Exhaustive grid search is a preferred method to determine the optimal solutions for stress tensor inversion because the object function can have multiple peaks. This study developed a uniform computational grid of normalised stress tensors. We designed the grid by using the reformulated parameter space, where normalised stress tensors correspond to points on the five-dimensional unit sphere. A computer-based procedure enabled us to arrange points on the sphere at approximately constant intervals. As a result, the new grid includes a greater number of triaxial stresses than axial stresses and their principal axes are uniformly distributed in physical space. An analysis of artificial fault-slip data using the multiple inverse method showed that the utilisation of the uniform grid enhanced the resolution in distinguishing stress tensors.
© 2006 Published by Elsevier Ltd.

Keywords: Uniform distribution; Hypersphere; Grid search; Stress tensor inversion; Fault-slip analysis

1. Introduction

In order to understand the palaeostress states in the earth's upper crust, we can use the stress tensor inversion of fault-slip data. Since the pioneering work by Carey and Brunier (1974), a variety of algorithms have been proposed for the inversion (e.g. Angelier, 1979; Etchecopar et al., 1981; Gephart and Forsyth, 1984; Nemcok and Lisle, 1995; Ramsay and Lisle, 2000, p. 797; Yamaji, 2000). Whether explicitly or implicitly, all methods utilise the objective function that evaluates the fitness or unfitness of some assumed stress tensor to the data. The optimal solution is indicated by the extremum value of the function. Therefore, the task comes down to a peak detection problem.

The majority of recent inversion techniques use the computational grid and examine all possible stress states. At the cost of calculation time and memory of the computing machine, the exhaustive grid search succeeds in finding the global optimum. If the fault-slip data are heterogeneous, the objective function has multiple peaks (Yamaji, 2003). The grid search method has another merit in the potential for detecting multiple stress states by, for example, enumerating local optima (Yamaji et al., 2006).

The design of computational grid inevitably affects the result. The grid should span over the solution space with a sufficient number density of grid points. Here arises a problem: what kind of solution space is suitable to express the variety of stress states? We employ the five-dimensional parameter space introduced by Sato and Yamaji (2006), which has been modified from Fry's (1999, 2001) σ-space. The reshaped parameter space has advantages in the simple geometry and in the metric equated to a measure of difference between stress states proposed by Orife and Lisle (2003). This study attempts to distribute the grid points uniformly in the parameter space at constant intervals. Although the random distribution is easier to generate, it is ineffective because the resolution is improved as slowly as the square root of the number of point. In contrast, a well-designed computational grid is effective (Matoušek, 1999).

In this article, we first point out a problem in the conventional grid. Then the uniform distribution of grid points is generated by a computer-based technique (Lovisolo and da Silva, 2001). A heterogeneous fault-slip dataset is analysed by the multiple inverse method (Yamaji, 2000) with the new grid to demonstrate the enhanced resolution in separating stresses.

2. Problem in the conventional grid

2.1. Reduced stress tensor

The Wallace–Bott hypothesis (Wallace, 1951; Bott, 1959) is the theoretical basis of recent stress tensor inversion

* Corresponding author. Tel.: +81-75-753-7531 (ext. 4173); fax: +81-75-753-4189.

E-mail address: k_sato@kueps.kyoto-u.ac.jp (K. Sato).

0191-8141/$ - see front matter © 2006 Published by Elsevier Ltd.
doi:10.1016/j.jsg.2006.03.007

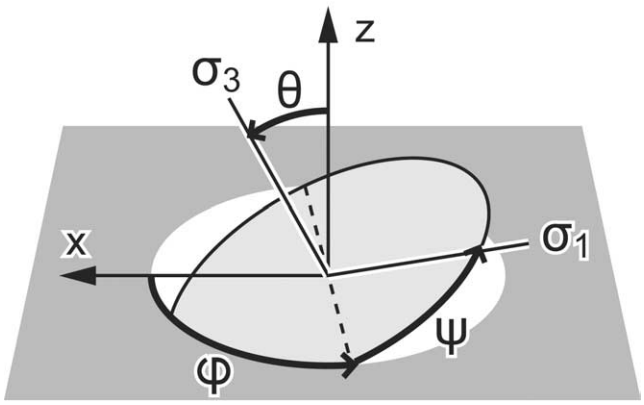

Fig. 1. Euler angles ϕ, θ and ψ, which describe the principal coordinate system. The σ_3-axis is designated by ϕ and θ, while ψ is the rotation angle around σ_3-axis, specifying σ_1- and σ_2-axes.

techniques, which assumes that a fault slips parallel to the resolved shear stress exerted by a common stress tensor for all or some portion of observed faults. Since the hypothesis requires only directional accordance, the inversion cannot constrain the magnitudes of stress. Therefore, we deal with the so-called reduced stress tensor (e.g. Angelier, 1984), which has four degrees of freedom.

The four unknowns can be specified by three Euler angles, ϕ, θ and ψ (Fig. 1), and the stress ratio

$$\Phi = (\sigma_2 - \sigma_3)/(\sigma_1 - \sigma_3), \tag{1}$$

where σ_1, σ_2 and σ_3 are the maximum, intermediate and minimum principal stress magnitudes, compression being positive. The value of Φ takes its minimum, 0, for an axial compressional stress ($\sigma_1 > \sigma_2 = \sigma_3$) and its maximum, 1, for an axial tensional stress ($\sigma_1 = \sigma_2 > \sigma_3$). Between the extremes, $0 < \Phi < 1$, the stress is triaxial.

A stress tensor has an alternative expression as a stress ellipsoid, of which principal radii directly represent the orientations and magnitudes of principal stresses (Fig. 2). The three Euler angles and the stress ratios describe the orientation and the shape of the ellipsoid, respectively.

2.2. Conventional grid

Hitherto, the computational grids of reduced stress tensors have been generated by changing the above-mentioned four parameters (e.g. Gephart and Forsyth, 1984; Nemcok and Lisle, 1995; Ramsay and Lisle, 2000, p. 797; Yamaji, 2000). The method of Yamaji (2000) attempted to give a uniform grid including 59,400 reduced stress tensors, which we refer to as the conventional grid.

First, 300 orientations of σ_3-axes are generated as a spiral set (Rakhmanov et al., 1994) on the hemisphere, which provides approximately uniform distribution on the three-dimensional sphere (Fig. 3a). The σ_3-axes can be specified by the Euler angles ϕ ($0 \le \phi < 2\pi$) as longitude and θ ($0 \le \theta \le \pi/2$) as colatitude (Fig. 1). Second, σ_1- and σ_2-axes are rotated on the plane perpendicular to each σ_3-axis. The rotation angle is indicated by ψ ($0 < \psi < \pi$, see Fig. 1), and is digitised into 18 values at regular intervals (Fig. 3b). In consequence, you get $300 \times 18 = 5400$ principal orientations. The average interval is 10°. Finally, 11 values of stress ratio Φ are assigned to each orientation. The interval of stress ratio is 0.1 from 0 to 1.

The conventional grid includes all possible reduced stress tensors and has a virtually uniform density in orientation. A set of three Euler angles is represented by a point in the 'Euler space', which takes ϕ, θ and ψ as orthogonal coordinates. Bunge (1985, pp. 81–86) has argued that the volume element of the space is given by

$$dv = \frac{1}{8\pi^2} \sin\theta d\phi d\theta d\psi. \tag{2}$$

If the number of points in the volume dv is constant, the density of orientations of three orthogonal axes is uniform. Since $\sin\theta d\phi d\theta$ represents the area element on the unit sphere, the spiral set (ϕ and θ) and regularly discretised ψ satisfies this condition.

However, we deal with the stress ellipsoid that is parameterised not only by the principal orientations but also by the shape parameter (stress ratio), Φ, and the problem of the conventional grid is in the independent generations of orientations and stress ratios. The variety of orientations of the ellipsoid actually depends on its own shape. For instance, suppose that we have a nearly axial tensional stress ($\Phi \approx 1$). The attitude of stress ellipsoid is almost completely described only by the orientation of σ_3-axis. Since the magnitudes of σ_1 and σ_2 are comparable, the rotation around σ_3-axis by the Euler angle ψ is less significant (Fig. 2c). From the viewpoint of degrees of freedom, axial stresses can be described by a single axis with two variables (e.g. longitude and colatitude). In contrast, a triaxial stress needs one more axis specified. Accordingly, triaxial stresses have more diversity in orientation than axial ones. Although the conventional grid contains the same number of tensors for each value of Φ, the uniform computational grid proposed in this paper is expected to include a greater number of tensors around $\Phi = 0.5$.

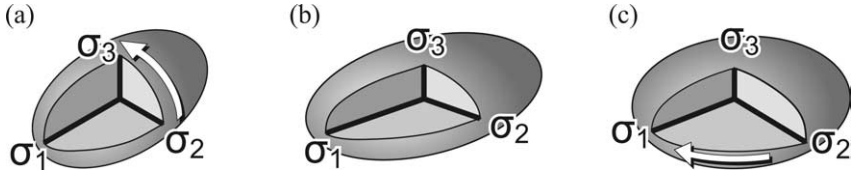

Fig. 2. Stress ratio and stress ellipsoid. (a) An axial compressional stress ($\Phi = 0$). (b) A triaxial stress ($0 < \Phi < 1$). (c) An axial tensional stress ($\Phi = 1$). Owing to the prolate and oblate shapes of stress ellipsoids, the rotations indicated by white arrows in (a) and (c) have no effect on the attitudes of ellipsoids or stress tensors.

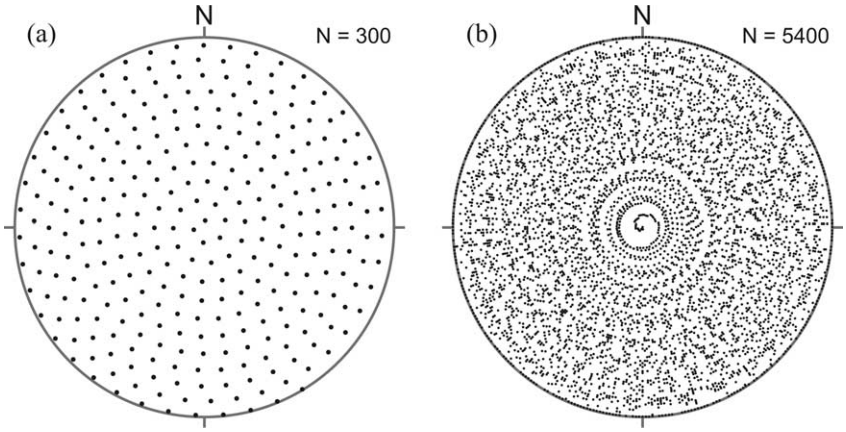

Fig. 3. Principal orientations included in the conventional grid. (a) σ_3-axes. (b) σ_1-axes. Both stereograms use equal-area and lower hemisphere projections. See text for the method of generating these orientations.

3. New computational grid

3.1. Theoretical basis

To obtain a uniform set of reduced stress tensors, we propose a new strategy. The parameter space for symmetric tensors (Sato and Yamaji, 2006) is utilised, which has been modified from the σ-space (Fry, 1999, 2001). In the parameter space, reduced stress tensors are represented by 'σ-vectors' with their end points on the five-dimensional unit sphere S_5. Note that a point on S_5 has four degrees of freedom similarly to a reduced stress tensor.

The Euclidean metric on S_5 corresponds to the stress difference D ($0 \leq D \leq 2$), which was proposed by Orife and Lisle (2003). D is a well-defined and convenient measure of difference between reduced stress tensors. Eventually, uniformly distributed points on S_5 give a set of reduced stress tensors spaced at regular intervals measured by the stress difference.

3.2. Generation of uniform computational grid

The problem of distributing many points uniformly over a (hyper-)sphere attracts widespread interests owing to its diverse applicability, although it generally has no analytic solution. Saff and Kuijlaars (1997) has plainly summarised this problem. Following the method of Lovisolo and da Silva (2001), we obtained an approximate uniformity of distributed points on the five-dimensional sphere. The procedure was divided into two parts. First, the 'square-tiling' method (Lovisolo and da Silva, 2001), as we called it, generated a passably uniform distribution. Second, the LBG algorithm (Linde et al., 1980) enhanced the uniformity.

Compared with the stochastic random generation, the square-tiling method achieves a far better uniformity of distributed points on a sphere. This method begins with setting the length of edge of the 'square', which is calculated from the surface area of sphere and the number of points to be distributed. Then points are generated, one by one, with the increments of spherical coordinates adjusted so as to keep the area of square constant in each step. We generated 60,000 points on S_5, which we call the 'initial set'.

The distribution of the 'initial set' was improved by the LBG algorithm, which is equivalent to the k-means clustering technique (MacQueen, 1967). A clustering method is usually employed to classify scattered points with some concentrated regions. Meanwhile, Lovisolo and da Silva (2001) applied the technique to a great number of points scattered uniformly, which are called the 'training set'. Although the uniformity of the training set is not sufficient, the resultant centres of clusters are expected to be arranged at a nearly regular interval, since there is no concentrated part to be specified.

The 60,000 points of the initial set were used as initial cluster centres. The 'training set' of 60,000,000 points (1000 times more than the initial set) was also generated by the square-tiling method. The LBG algorithm classified the training set into 60,000 clusters. The cluster centres were interpreted as σ-vectors and converted to reduced stress tensors according to the formulation of Sato and Yamaji (2006). The calculation took some 8 h with 32 CPUs of a parallel scalar supercomputer at Kyoto University.

4. Features of the uniform grid

4.1. Test of uniformity

This subsection examines the geometrical uniformity of the present computational grid of five-dimensional points. Firstly, the mean vector $\langle\vec{\sigma}\rangle$ and the covariance matrix $\mathbf{V}$ of the 60,000 points were calculated:

$$\langle\vec{\sigma}\rangle = (-0.0005,\ 0.0003,\ -0.0000,\ 0.0000,\ -0.0006)^{\mathrm{T}},$$

$$\mathbf{V} = \begin{pmatrix} 0.1953 & 0.0004 & 0.0002 & -0.0000 & -0.0000 \\ & 0.1983 & 0.0003 & -0.0001 & 0.0001 \\ & & 0.2008 & 0.0000 & 0.0001 \\ & & & 0.2029 & 0.0001 \\ \text{symm.} & & & & 0.2026 \end{pmatrix},$$

where we omitted the symmetric part of **V** by noting 'symm.'. The mean vector almost coincides with the origin of parameter space and the covariance satisfies $\mathbf{V} \approx 1/5\mathbf{I}$, where **I** is the five-dimensional unit tensor. They demonstrate isotropic characteristics around the origin, which are the necessary conditions for a uniform distribution.

Second, we measured the distances between neighbouring grid points that are expected to be constant. Fig. 4 shows the frequency histograms of Euclidean distances between each grid point and its nearest neighbour. Note that the Euclidean distances in our parameter space represent the stress differences between corresponding reduced stress tensors (Section 3.1).

As for the conventional grid of 59,400 tensors (Fig. 4a), the nearest distances are relatively small and widely spread. The

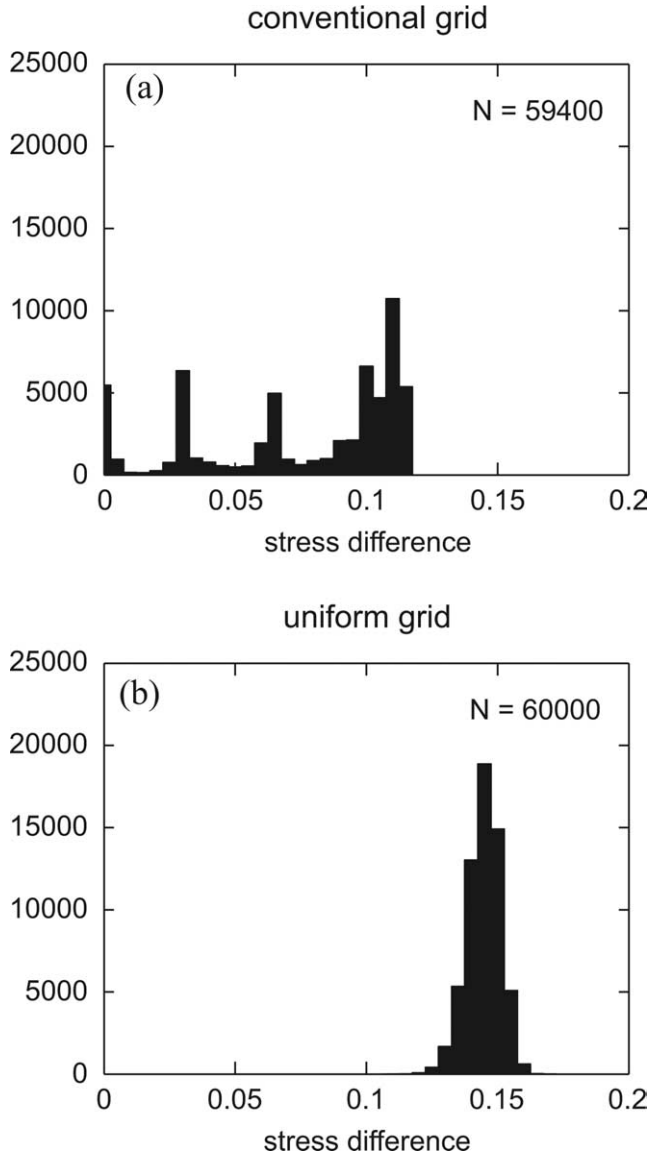

Fig. 4. Histograms of Euclidean distances between grid points and their nearest neighbours. Note that the distance is equivalent to the stress difference between corresponding reduced stress tensors. (a) The conventional grid shows a widely spread distribution showing non-uniformity. (b) The uniform grid has approximately regular intervals of 0.145 in stress difference.

average is 0.075 ± 0.039, where the uncertainty is the standard deviation. It was found that even identical tensors (null distance to their neighbours) were included in the conventional grid, which could be attributed to the meaningless rotation around the principal axis of an axial stress state (Fig. 2a and c).

The nearest Euclidean distances in the uniform computational grid are approximately constant (Fig. 4b). The average distance is 0.145 ± 0.006, which corresponds to the angular distance of $8.3 \pm 0.3°$ on the unit sphere S_5. The spread of these distances is not satisfactorily small, which can be ascribed to the lack of training points. Lovisolo and da Silva (2001) used a 1000 times larger number of training points than that of initial points for only a three-dimensional distribution, while our problem is five-dimensional. Since the increase of number of points requires much larger computing resources, we could not use enough training points. Setting aside this problem, the uniformity of the new grid is far better than that of the conventional one.

4.2. Contained stress tensors

Some favourable features were found from the reduced stress tensors contained in the uniform grid. Fig. 5 shows its orientational uniformity. The σ_1-axes of axial compression ($0 \leq \Phi \leq 0.1$), triaxial stress ($0.49 \leq \Phi \leq 0.51$) and axial tension ($0.9 \leq \Phi \leq 1$) were plotted on the stereograms of Fig. 5a–c, respectively. All these axes are almost uniformly distributed, even though the orientation in physical space was not considered in the generation of the uniform grid. The σ_1 orientation is more important for an axial compressional stress than for an axial tensional stress. Reflecting on that, the σ_1-axes in Fig. 5a appear to be distributed more uniformly than those in Fig. 5b and c.

The uniform grid includes the entire range of stress ratios ($0 \leq \Phi \leq 1$). Their frequency is unimodal and symmetric about the mode $\Phi = 0.5$ (Fig. 6). This abundance of triaxial stresses arises from their diversity in orientation, as was expected in Section 2.2. Again, this feature was not planned, but is a consequence of the expression of reduced stress tensors as points on the five-dimensional unit sphere.

4.3. Uniform frequency of angular misfit

Another way of evaluating the computational grid is to calculate the fitness to a single fault for each contained reduced stress tensor. Fig. 7 shows the frequency histograms of angular misfits between the slip direction of an arbitrary fault datum and the resolved shear stresses calculated for all reduced stresses. Compared with the conventional grid (Fig. 7a), the uniform grid (Fig. 7b) yielded a relatively uniform frequency. Since the angular misfit is often used to assess the determined stress through inversion, there should be no preferred value of angular misfit. The uniformity of the present grid justifies various algorithms of inversion using the angle as the objective function.

The above feature can be explained with the geometry in the parameter space. Sato and Yamaji (2006) have pointed out that

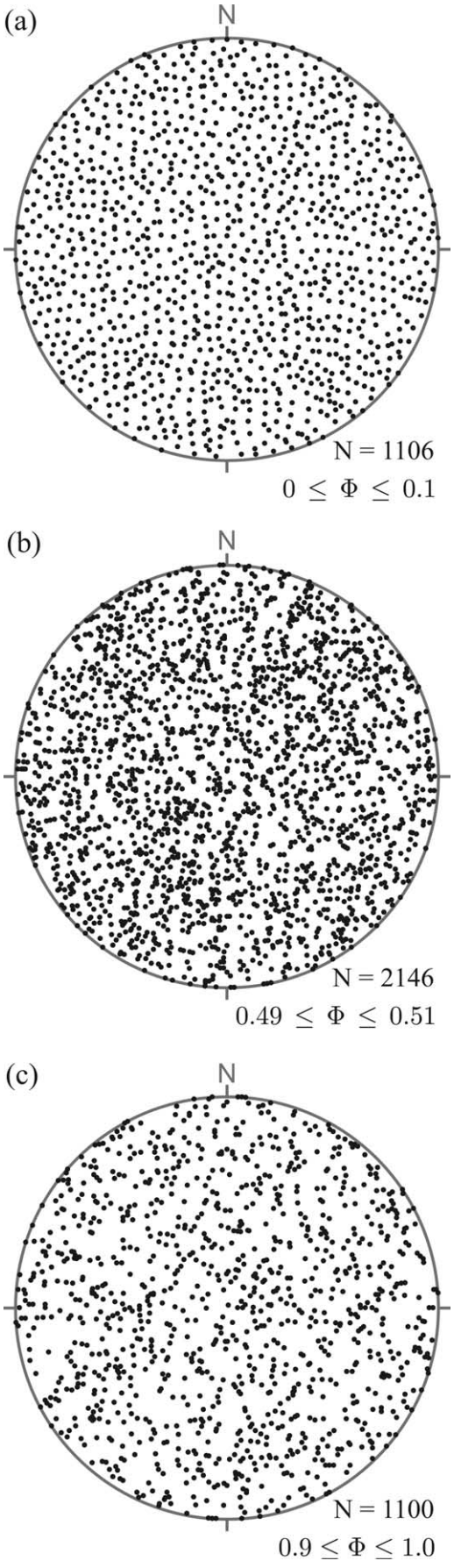

Fig. 5. Orientations of σ_1-axes in the uniform grid for each range of stress ratio. Since the orientation of σ_1-axis is more important for a lower value of stress ratio Φ, i.e. axial compression, the distribution has better uniformity with low Φ. (a) $0 \leq \Phi \leq 0.1$. (b) $0.49 \leq \Phi \leq 0.51$. (c) $0.9 \leq \Phi \leq 1$.

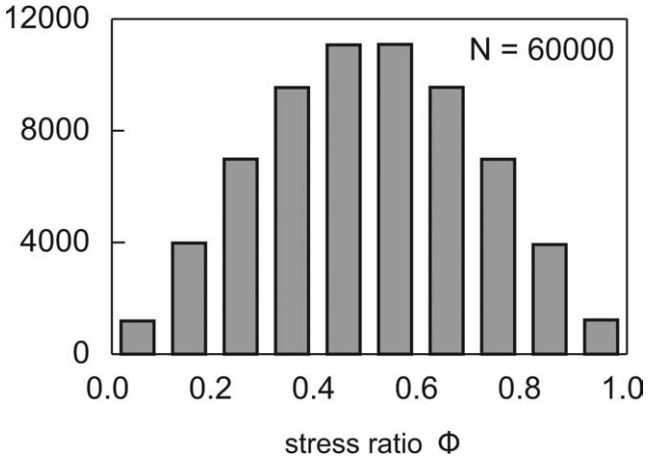

Fig. 6. Histogram of stress ratios of reduced stress tensors contained in the uniform grid. They show a unimodal distribution around the mode of $\Phi = 0.5$. Note that the conventional grid has, in contrast, the same number of grid points for each value of discretised stress ratio.

the angular misfit appears on the five-dimensional unit sphere S_5 as is shown in Fig. 8. A fault-slip datum is represented by the paired unit vectors $\vec{\varepsilon}$ and $\vec{\varepsilon}'$, which are perpendicular to each other (see Sato and Yamaji (2006) for details). When a σ-vector $\vec{\sigma}$ is orthogonally projected onto a two-dimensional $\vec{\varepsilon} - \vec{\varepsilon}'$ plane, the angle between the projected σ-vector $\vec{\sigma}^*$ and $\vec{\varepsilon}$ is equivalent to the angular misfit in physical space. On this geometry, a certain value of angular misfit is given by σ-vectors on a half great circle which meets $\vec{\varepsilon}$ at the angle. Owing to the uniformity of the present grid, all great semicircles include almost a constant number of trial σ-vectors. Accordingly, the angular misfits of stresses to any fault obey the uniform distribution.

5. Numerical experiment

5.1. Method

The practical effect of the newly developed grid was tested by using it as a search grid for stress tensor inversion. The analysed artificial fault-slip data are comprised of 60 faults (Fig. 9). The fault planes are randomly oriented and the slip directions are concordant with two stress states, both of which are triaxial ($\Phi = 0.5$). A NNE–SSW compressional stress (stress A) is responsible for 40 faults, while the remaining 20 faults result from N–S compression (stress B):

Stress A : σ_1 035/20, σ_3 125/00, $\Phi = 0.5$, 40 faults,

Stress B : σ_1 000/20, σ_3 090/00, $\Phi = 0.5$, 20 faults,

Therefore, the data are heterogeneous and stress A is easier to be detected than stress B owing to the large number of faults.

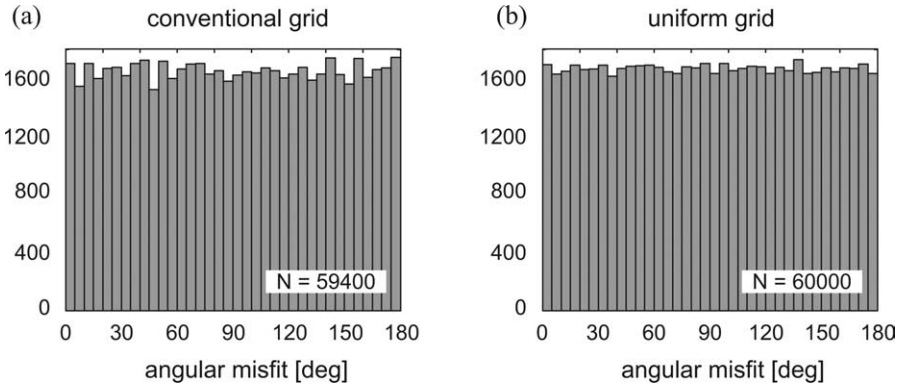

Fig. 7. Frequency histogram of angular misfit of stress tensors included in each grid against an arbitrary chosen fault-slip datum. (a) The conventional grid. (b) The uniform grid. The latter gives more uniform frequency of angular misfit.

We used the multiple inverse method (Yamaji, 2000) to separate these stresses. The method is a kind of resampling technique. After extracting all possible combinations of k faults from the whole dataset of N faults, where we set $k=4$, the optimal reduced stress tensors are determined for each subset. The number of solutions is given by the binomial coefficient ${}_NC^N = N!/k!(N-k)!$. The significant stress states are recognised as clusters of the numerous solutions. This method uses the exhaustive grid search in determining the optimal solution for each subset and we tested the conventional grid of 59,400 tensors and the uniform grids of 60,000 and 30,000 tensors. The grid of 30,000 tensors was generated in the same procedure to that of 60,000 points. The software of the multiple inverse method with the uniform computational grid attached (Version 4.0 and later) is available to the public at our website (http://www.kueps.kyoto-u.ac.jp/~yamaji/PDS/indexe.html).

5.2. Results

The results of inversion are visualised in Fig. 10. Following Yamaji (2000), a reduced stress tensor was plotted as a tadpole-like symbol. The σ_1-axes are shown by 'heads' (squares) in each left-hand stereogram. The lengths and directions of the attached 'tails' (bars) represent the orientations of σ_3-axes, as if there were small stereograms around the heads. The right-hand stereograms are complementary ones in which the role of head and that of tail are interchanged. The greyscale colours indicate the values of stress ratio. In order to emphasise clusters,

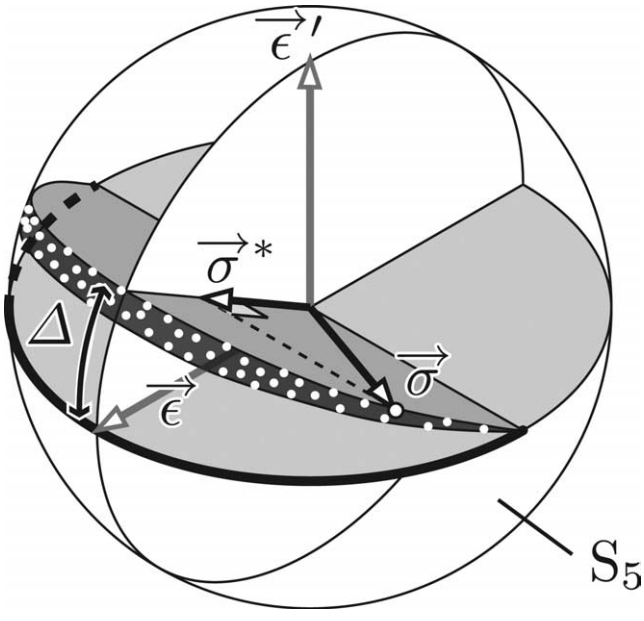

Fig. 8. Schematic figure showing the angular misfit Δ measured on the five-dimensional sphere S_5. A reduced stress tensor is equivalent to a σ-vector $\vec{\sigma}$. When $\vec{\sigma}$ is projected onto the $\vec{\varepsilon}-\vec{\varepsilon}'$ plane, which is specified by a fault-slip datum, the angle between $\vec{\varepsilon}$ and the projected vector $\vec{\sigma}^*$ is equal to the angular misfit. Therefore, σ-vectors shown by white dots give the same angle of misfit. On the half great circle shown by the bold line, the angular misfit equals zero. See Sato and Yamaji (2006) for detailed formulation.

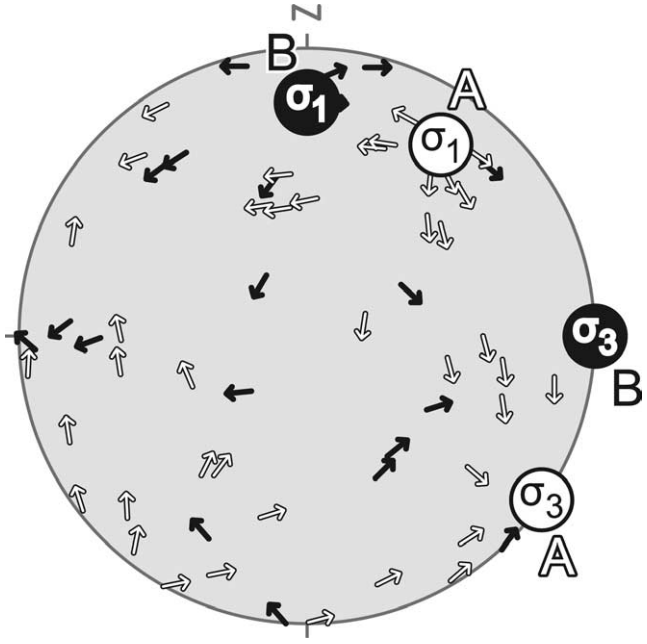

Fig. 9. Artificial fault-slip data used in the numerical experiment. The data are shown by the tangent-lineation diagram (Twiss and Gefell, 1990) with equal-area and lower hemisphere projections. The arrows are plotted in the positions of fault normals. They point to the slip directions of footwall blocks. The black and white arrows correspond to faults activated by stress A (40 faults) and stress B (20 faults), respectively.

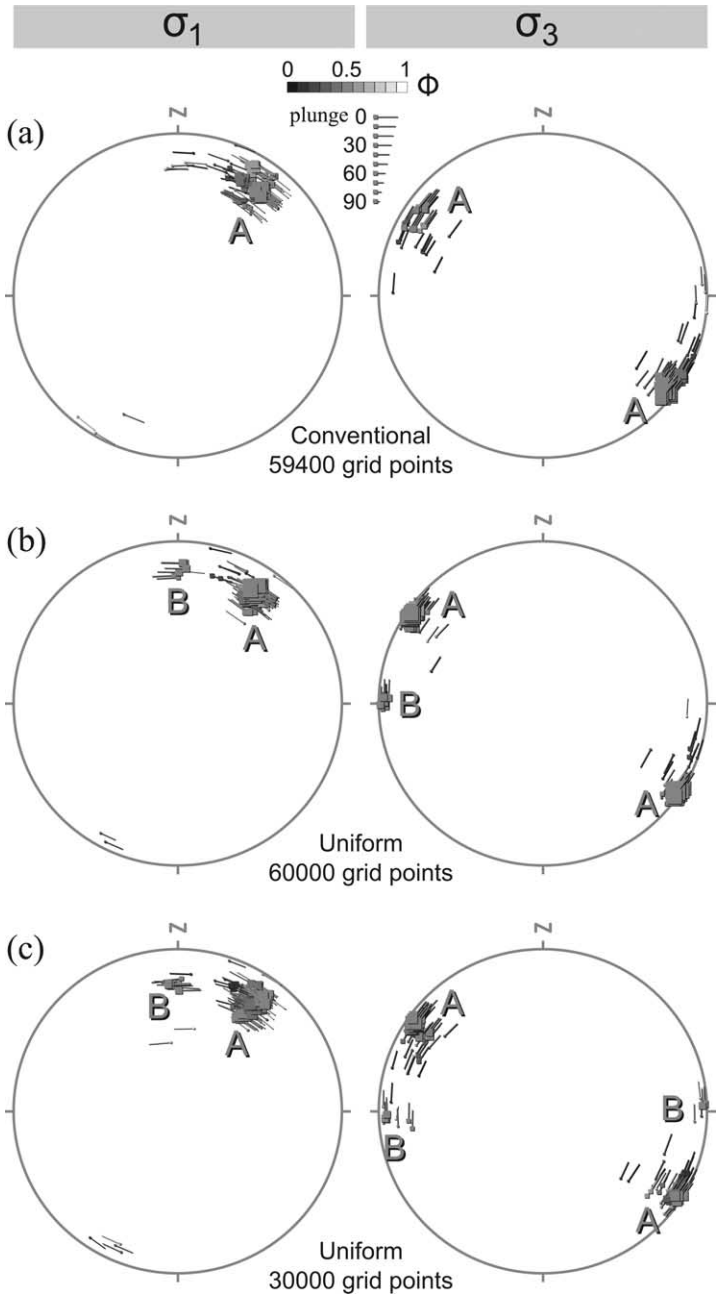

Fig. 10. The results of analyses by the multiple inverse method. (a) Using the conventional search grid (59,400 grid points), stress B of N–S compression cannot be detected. (b) The uniform search gird (60,000 grid points) successfully distinguished two stresses. (c) Even when the number of uniform grid points is reduced to 30,000, the given two stresses could be recognised. See text for the method of plotting stress tensors on the paired stereograms.

the 'heads' are enlarged according to their number of times selected as optimal solutions.

Using the conventional grid (Fig. 10a), the stress A of 40 faults was detected as a large cluster, while the stress B made so small a cluster that it could not be recognised. In contrast, the uniform grid enabled us to identify both stress states clearly (Fig. 10b). These results show the enhanced resolution in detecting plural stresses. Furthermore, the inversion on the uniform grid of 30,000 tensors also successfully distinguished two stresses (Fig. 10c). The calculation time for this case was about one-third of that with 60,000 grid points. Therefore, the computational efficiency was also improved.

The uniformity of computational grid is especially important for the multiple inverse method. Fig. 11 schematically shows the problem of a non-uniform grid. Assume that the extracted subsets of fault-slip data have their own optimal solutions irrespective of the arrangement of grid points. The solutions will be assigned to each nearest grid point. If the grid is coarse, the solutions are concentrated on a few grid points. Conversely, a fine grid will divide the solutions into many grid points, even if there is a potential cluster. Therefore, a non-uniform computational grid makes the resolution heterogeneous in solution space.

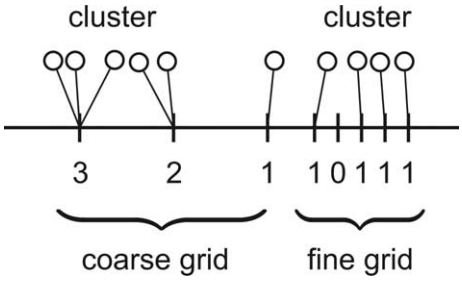

Fig. 11. Schematic figure showing the problem of a non-uniform search grid. The open circles are the optimal stresses for subsets of fault-slip data extracted by the multiple inverse method (Yamaji, 2000). For the coarse part of the search grid, the solutions are densely assigned, while the grid points in the fine part obtain small numbers of solutions. This heterogeneity distorts the resolution in detecting plural clusters of stresses.

6. Conclusion

The uniform computational grid of normalised stress tensors was developed. The uniformity is defined in the parameter space (Sato and Yamaji, 2006), where a reduced stress tensor is equivalent to a point on the five-dimensional unit sphere and the metric corresponds to the stress difference (Orife and Lisle, 2003). The computer-based technique of Lovisolo and da Silva (2001) generated the uniformly distributed points on the hypersphere. When the new grid is used as a search grid for the multiple inverse method (Yamaji, 2000), the resolution in detecting plural stresses is enhanced. The uniform computational grid has potential application to the inversion of other physical quantities represented by symmetric and normalised tensors and may be useful for theoretical investigations on such tensor quantities.

Acknowledgements

The authors thank Norman Fry and Richard Lisle for their careful reviews on the manuscript. This work was supported by Kyoto University Active Geosphere Investigations for the 21st Century Centers of Excellence Program (KAGI21) and by the Japan Society for the Promotion of Science (No. 14540423).

References

Angelier, J., 1979. Determination of the mean principal directions of stresses for a given fault population. Tectonophysics 56, T17–T26.

Angelier, J., 1984. Tectonic analysis of fault slip data sets. Journal of Geophysical Research 89, 5835–5848.

Bott, M.H.P., 1959. The mechanics of oblique slip faulting. Geological Magazine 96, 109–117.

Bunge, H.J., 1985. Representation of preferred orientations. In: Wenk, H. (Ed.), Preferred Orientation in Deformed Metals and Rocks: an Introduction to Modern Texture Analysis. Academic Press, Orland, pp. 73–108.

Carey, M.E., Brunier, M.B., 1974. Analyse théorique et numérique d'un modèle mécanique élémentaire appliqué à l'étude d'une population de failles. Compte Rendus de l'Académie des Sciences 279, 891–894.

Etchecopar, A., Vasseur, G., Daignieres, M., 1981. An inverse problem in microtectonics for the determination of stress tensors from fault striation analysis. Journal of Structural Geology 3, 51–65.

Fry, N., 1999. Striated faults: visual appreciation of their constraint on possible paleostress tensors. Journal of Structural Geology 21, 7–21.

Fry, N., 2001. Stress space: striated faults, deformation twins, and their constraints on paleostress. Journal of Structural Geology 23, 1–9.

Gephart, J.W., Forsyth, D.W., 1984. An improved method for determining the regional stress tensor using earthquake focal mechanism data—application to the San-Fernando earthquake sequence. Journal of Geophysical Research 89, 9305–9320.

Linde, Y., Buzo, A., Gray, R.M., 1980. Algorithm for vector quantizer design. IEEE Transactions on Communications 28, 84–95.

Lovisolo, L., da Silva, E.A.B., 2001. Uniform distribution of points on a hypersphere with applications to vector bit-plane encoding. IEE Proceedings—Vision, Image and Signal Processing 148, 187–193.

MacQueen, J., 1967. Some methods for classification and analysis of multivariate observations. Proceedings of the Fifth Berkeley Symposium on Mathematical Statistics and Probability 1, 281–296.

Matoušek, J., 1999. Geometric Discrepancy: an Illustrated Guide. Vol. 18 of Algorithms and Combinatorics. Springer, Berlin.

Nemcok, M., Lisle, R.J., 1995. A stress inversion procedure for polyphase fault/slip data sets. Journal of Structural Geology 17, 1445–1453.

Orife, T., Lisle, R.J., 2003. Numerical processing of palaeostress results. Journal of Structural Geology 25, 949–957.

Rakhmanov, E.A., Saff, E.B., Zhou, Y.M., 1994. Minimal discrete energy on the sphere. Mathematical Research Letters 1, 647–662.

Ramsay, J.G., Lisle, R.J., 2000. Applications of Continuum Mechanics in Structural Geology. Vol. 3: The Techniques of Modern Structural Geology. Academic Press, San Diego.

Saff, E.B., Kuijlaars, A.B.J., 1997. Distributing many points on a sphere. Mathematical Intelligencer 19, 5–11.

Sato, K., Yamaji, A., 2006. Embedding stress difference in parameter space for stress tensor inversion. Journal of Structural Geology, this special issue, doi.: 10.1016/j.jsg.2006.03.004.

Twiss, R.J., Gefell, M.J., 1990. Curved slickenfibers—a new brittle shear sense indicator with application to a sheared serpentinite. Journal of Structural Geology 12, 471–481.

Wallace, R.E., 1951. Geometry of shearing stress and relation to faulting. Journal of Geology 59, 118–130.

Yamaji, A., 2000. The multiple inverse method: a new technique to separate stresses from heterogeneous fault-slip data. Journal of Structural Geology 22, 441–452.

Yamaji, A., 2003. Are the solutions of stress inversion correct? Visualization of their reliability and the separation of stresses from heterogeneous fault-slip data. Journal of Structural Geology 25, 241–252.

Yamaji, A., Otsubo, M., Sato, K., 2006. Paleostress analysis using the Hough transform for separating stresses from heterogeneous fault-slip data. Journal of Structural Geology, this special issue, doi.: 10.1016/j.jsg.2006.03.016.